ISSN 0023-1584, Kinetics and Catalysis, 2012, Vol. 53, No. 4, pp. 425–439. © Pleiades Publishing, Ltd., 2012.
Original Russian Text © A.S. Ivanova, 2012, published in Kinetika i Kataliz, 2012, Vol. 53, No. 4, pp. 446–460.

Aluminum Oxide and Systems Based on It: Properties and Applications

A. S. Ivanova

Boreskov Institute of Catalysis, Siberian Branch, Russian Academy of Sciences, Novosibirsk, 630090 Russia

e-mail: iva@catalysis.ru

Received December 21, 2011

Abstract—The metastable forms of aluminum oxide that exist in the range of 300–800°C are characterized; differences in the microstructures of homogeneous γ-, η-, and χ-Al_2O_3 are demonstrated; and the acid–base properties of the above modifications are compared. The catalytic properties of aluminum oxide in ethanol dehydration and propionitrile ammonolysis were studied. It was found that an increased surface concentration of Lewis acid sites, including strong acid sites ($\nu(CO) = 2237$ cm^{-1}), is required for preparing an effective catalyst for the dehydration of ethanol, whereas the rate of propionitrile conversion increased proportionally to the surface concentration of Brønsted acid sites. γ-Aluminum oxide was used to prepare catalysts for carbon monoxide oxidation. It was found that the supporting of Pd on γ-Al_2O_3 did not change the support structure. Palladium on the surface of γ-Al_2O_3-550 ($T_{calcin} = 550$°C, $S_{BET} = 300$ m^2/g) occurred as single particles (2–3 nm) and aggregates (~100 nm). The single particles were almost completely covered with a layer of aluminum oxide to form core–shell structures. According to XPS data, they were in atypical states (BE(Pd $3d_{5/2}$) = 336.0 and 338.0 eV), which were not reduced by hydrogen in the range of 15–450°C and were resistant to the action of the reaction mixture. Palladium on the surface of γ-Al_2O_3-800 ($S_{BET} = 160$ m^2/g) was in the states Pd^0 and PdO, which are typical of Pd/Al_2O_3, and the proportions of these states can change under the action of the reaction mixture. An increase in the T_{calcin} of the Pd/Al_2O_3(800)-450 catalyst from 450 to 800 → 1000 → 1200°C led to the agglomeration of palladium particles and to an increase in the temperature of 50% CO conversion from 145 to 152 → 169 → 189°C, respectively. α-Aluminum oxide was used in the preparation of an effective Mn–Bi–O/α-Al_2O_3 supported catalyst for the synthesis of nitrous oxide by the oxidation of ammonia with oxygen: the NH_3 conversion was 95–97% at 84.4% N_2O selectivity.

DOI: 10.1134/S0023158412040039

PHYSICOCHEMICAL PRINCIPLES OF THE SYNTHESIS OF ALUMINUM HYDROXIDE

Because of its unique properties, aluminum oxide has been widely used in catalysis for a long time, and the annual world output of aluminum oxide and systems based on it exceeds 115 million tons.

Aluminum oxide is used as a catalyst in the dehydration of alcohols [1], in the Claus process [1, 2], in the cracking and hydrocracking reactions of petroleum products [3, 4], etc.; as a component for the synthesis of complex catalysts (chromium–alumina, alumina–molybdenum, alumina–cobalt–molybdenum, and alumina–nickel–molybdenum) [5]; and as a support for supported metal (Pt, Pd, and Ni) and oxide catalysts, which are used in hydrogenation, hydrogenolysis, reforming, etc., [6] and also in the neutralization of industrial waste [7–12].

The widest use of aluminum oxide is due to the structural features of its modifications (γ-, η-, χ-, δ-, θ-, κ-, and α-Al_2O_3), which, in turn, determine the particle size of the oxide and the state of its surface. The main characteristics of aluminum oxide (amount and nature of impurities, phase composition, acid–base surface properties, specific surface area, pore volume, pore-size distribution, and mechanical properties) are governed by the structure and morphology of the initial hydroxide, which, in turn, depend on the preparation conditions. The existing modifications of aluminum hydroxide, their structural features, preparation methods, and main properties were considered in detail elsewhere [13]. Note that, among the various methods for the preparation of aluminum hydroxide, precipitation is most widely used in the domestic practice; this method makes it possible to vary the chemical and phase composition, morphology, particle size, and texture characteristics of the resulting aluminum hydroxide and aluminum oxide by changing pH, precipitation temperature, aging time (τ), and the nature of the precipitating agent.

The following was demonstrated:

(1) Aluminum hydroxide prepared at low temperatures and pH values contains a significant amount of an amorphous phase; it is moldable and undergoes changes in time (precipitate aging). The rate of the

conversion of the amorphous precipitate into the crystalline state increases with increasing temperature and the pH of suspension; at elevated temperatures and pH 7–9, pseudoboehmite is mainly crystallized, whereas bayerite is mainly crystallized at low temperatures and pH ≥ 10–10.5. The rates of crystallization of pseudoboehmite and bayerite depend mainly on the precipitation temperature and the pH of precipitation, respectively [14, 15].

(2) The qualitative characteristics of aluminum hydroxide depend on the nature of the initial reagents because the basic salts forming during precipitation have different rates of hydrolysis. All of the factors that facilitate the most complete hydrolysis and the removal of cations and anions lead to an increase in the specific surface area. To obtain aluminum hydroxide with the largest specific surface area, the precipitation should be performed at pH 7–9 and a temperature of ≥ 70°C; however, these precipitates are difficult to filter off.

(3) An increase in the pH of precipitation facilitates an increase in the porosimetric volume and a decrease in the bulk weight and mechanical strength of aluminum hydroxide.

ALUMINUM OXIDES

Aluminum oxides are usually prepared by the dehydration of the corresponding hydroxide modifications on heating. The thermal genesis of aluminum hydroxide depends on a number of factors—aluminum hydroxide preparation conditions, homogeneity, chemical purity, and particle size—that is, on the entire prehistory of aluminum hydroxide preparation. At $T \geq 300$°C, the dehydration of aluminum hydroxide occurs, but the resulting oxides contain a small amount of constitution water, which is gradually removed on heating; however, its concentration even at 1000°C is several tenths of a percent, which is consistent with published views [16]. The dehydration of various aluminum hydroxide modifications can be schematically represented as follows [17–24]:

$$\text{amorphous} \xrightarrow{700^\circ\text{C}} \eta\text{-} \xrightarrow{1150^\circ\text{C}} \alpha\text{-}Al_2O_3,$$

$$\text{pseudoboehmite} \xrightarrow{300^\circ\text{C}} \gamma\text{-} \xrightarrow{900^\circ\text{C}} \delta\text{-} \xrightarrow{1000^\circ\text{C}} \theta\text{-} + \alpha\text{-} \xrightarrow{1200^\circ\text{C}} \alpha\text{-}Al_2O_3,$$

$$\text{boehmite} \xrightarrow{450^\circ\text{C}} \gamma\text{-} \xrightarrow{600^\circ\text{C}} \delta\text{-} \xrightarrow{1050^\circ\text{C}} \theta\text{-} + \alpha\text{-} \xrightarrow{1200^\circ\text{C}} \alpha\text{-}Al_2O_3,$$

$$\text{bayerite} \xrightarrow{230^\circ\text{C}} \eta\text{-} \xrightarrow{850^\circ\text{C}} \theta\text{-} \xrightarrow{1200^\circ\text{C}} \alpha\text{-}Al_2O_3,$$

$$\text{bayerite} \xrightarrow{200^\circ\text{C}} \text{boehmite} \xrightarrow{510^\circ\text{C}} \gamma\text{-} \xrightarrow{750\text{–}900^\circ\text{C}} \delta\text{-} \xrightarrow{1050^\circ\text{C}} \theta\text{-} + \alpha\text{-} \xrightarrow{1200^\circ\text{C}} \alpha\text{-}Al_2O_3,$$

$$\text{gibbsite} \xrightarrow{180^\circ\text{C}} \text{boehmite}$$

$$\text{gibbsite} \xrightarrow{250^\circ\text{C}} \chi\text{-} \xrightarrow{900^\circ\text{C}} \kappa\text{-} \xrightarrow{1200^\circ\text{C}} \alpha\text{-}Al_2O_3.$$

Note that the γ-Al_2O_3 samples forming from pseudoboehmite (H_2O/Al_2O_3 = 1.52 mol/mol, S_{BET} = 420 m^2/g) and boehmite (H_2O/Al_2O_3 = 1.06 mol/mol, S_{BET} = 2 m^2/g) are structurally different [19]. γ-Al_2O_3 prepared from pseudoboehmite consists of aggregates (>100 nm) of fine (~2 nm) oxide particles, which are nonoriented and located at large angles relative to one another. γ_{boe}-Al_2O_3 prepared from boehmite consists of particles as extensive (~100 nm) thin single-crystal plates whose most developed face is {110}. The main feature of these particles is specifically closed defects [25] formed by extensive dislocation walls as a result of the coalescence of lattice vacancies upon structure formation. Therefore, γ- and γ_{boe}-Al_2O_3 are microstructurally different, while they have the same defective spinel structure.

The above scheme indicates that bayerite and gibbsite can be dehydrated according to two reaction paths, depending on their particle size. It was found [26–28] that small bayerite and gibbsite particles are dehydrated directly to η- and χ-Al_2O_3, respectively; however, conditions ensuring excess water vapor or intraglobular hydrothermal conditions are generated in large trihydroxide particles to facilitate the formation of boehmite. Kul'ko et al. [27] determined the conditions under which homogeneous η- and χ-Al_2O_3 are formed.

According to electron microscopic data, the particles of η-Al_2O_3 are thin (20 nm) plates combined into aggregates (Fig. 1a). The microdiffraction pattern contains point reflections, which indicate that an individual single-crystal plate with a developed [110] plane includes particles with a developed [111] plane of the oxide structure. The particles of homogeneous χ-Al_2O_3 are morphologically similar to the above particles of η-Al_2O_3 (Fig. 1b); however, their microdiffraction pattern is annular, which is indicative of the polycrystalline nature of the structure of χ-Al_2O_3. This can be explained by the fact that the individual plates consist of nonoriented microblocks. This leads to the transformation of point reflections into annular reflections, which are analogous to those observed for polycrystalline aggregates. The microstructure of homogeneous η-Al_2O_3 prepared by the dehydration of bayerite at 600°C consists of particles whose most developed face is {111}; these particles are composed of coherently joined domains with a clearly pronounced lamellar shape (Fig. 2a). The particles contain a system of planar defects (boundaries with a strictly definite orientation) located in the [111] plane (Fig. 2b).

Thus, the low-temperature aluminum oxides (γ-, γ_{boe}-, and η-Al_2O_3), having the same spinel structure, are essentially different in terms of microstructure; this fact can affect their surface properties.

ACID–BASE PROPERTIES OF ALUMINUM OXIDES

The chemical nature of the surface of aluminum oxide is mainly responsible for its catalytic and adsorp-

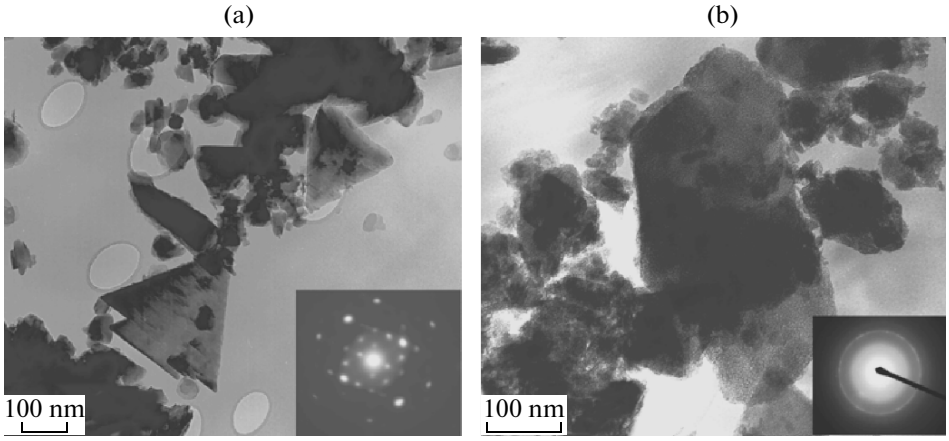

Fig. 1. Electron micrographs of (a) η-Al_2O_3 (600°C) and (b) χ-Al_2O_3 (600°C).

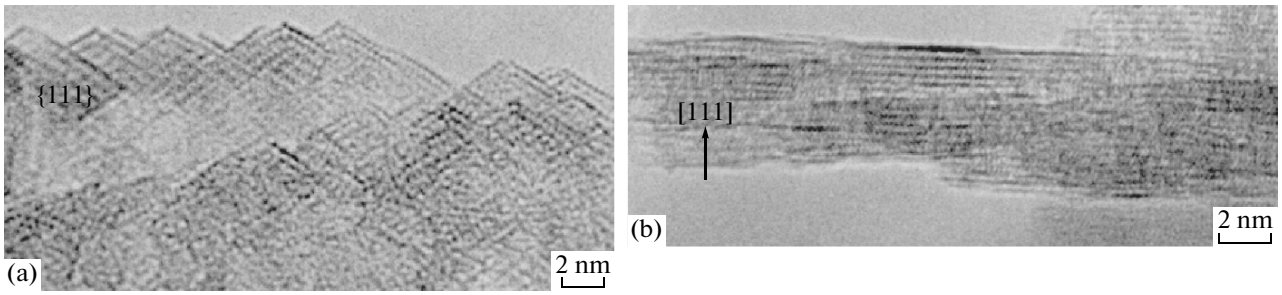

Fig. 2. Micrograph of a particle of η-Al_2O_3: (a) the developed [111] plane and (b) planar defects in planes perpendicular to [111].

tion properties. According to current views, the surface of aluminum oxide at room temperature is occupied by OH groups or water molecules coordinated to aluminum and oxygen ions. Surface dehydration and dehydroxylation lead to the appearance of the coordinatively unsaturated atoms of oxygen (Lewis base) and aluminum (Lewis acid) [29–31]. It is well known [32] that five types of OH groups with different configurations of the nearest neighbors can occur on the dehydroxylated surface of Al_2O_3. Their properties depend on the structure of the fragment to which they are bound [4, 31, 33]: the OH group bound to aluminum in a tetrahedral coordination environment (terminal group) is the most basic, whereas the OH group located between two aluminum ions in tetrahedral and octahedral environments (bridging group) is the most acidic. The removal of OH groups from the surface of Al_2O_3 in the course of dehydration is regulated by the relative acidity and basicity of adjacent OH groups.

Many publications have been devoted to the acid–base properties of aluminum oxide [4, 29–32, 34, 35]. However, the degrees of homogeneity of particular oxides and the effect of the presence of another phase on the acid–base properties were not considered. Since particular modifications of homogeneous aluminum oxides were obtained [19, 27], it became possible to compare their acid–base properties. Table 1 summarizes the structure and texture characteristics of the homogeneous aluminum oxides. It is evident that they differ not only in structure but also in specific surface areas.

The study of the above aluminum oxides by IR spectroscopy showed [36] that the spectrum of their hydroxyl cover contains five to eight absorption bands due to terminal, bridging, and hydrogen-bonded OH groups. The total concentrations of the terminal (C_t) (absorption bands at 3795–3758 cm^{-1}) and bridging (C_b) (absorption bands at 3735–3670 cm^{-1}) OH groups per square meter of the surface area decrease in different orders.

Al_2O_3	χ-	γ-	γ_{boe}-	η-	θ-
C_t, $\mu mol/m^2$	0.52	0.51	0.46	0.19	0.16
Al_2O_3	γ_{boe}-	γ-	χ-	θ-	η-
C_b, $\mu mol/m^2$	1.76	1.36	0.58	0.60	0.53

The hydrogen-bonded OH groups occur only in γ- and γ_{boe}-Al_2O_3, and their concentration is low. An analysis of the above orders shows that, among the aluminum oxides, γ_{boe}-Al_2O_3 is characterized by the high-

Table 1. Main characteristics of homogeneous aluminum oxides [36]

Hydroxide	Na	Fe	Si	H_2O/Al_2O_3, mol/mol	S_{BET}, m^2/g	T_{calcin}, °C	Aluminum oxide	
	wt %						Al_2O_2 phase	S_{BET}, m^2/g
Pseudoboehmite	<0.001	0.001	0.02	1.52	420	600	γ-	220
Boehmite	–	0.024	0.57	1.06	2	600	γ_{boe}-	90
Bayerite	–	<0.001	0.08	2.99	38	600	η-	300
						1000	θ-	106
Gibbsite	0.180	0.020	–	2.92	16	600	χ-	260

Table 2. Positions of the absorption bands of LAS's in the IR spectra of aluminum oxide samples and the concentrations of adsorbed CO on LAS's [36]

Al_2O_3 sample	ν(CO), cm^{-1}			ΣLAS, μmol/g (μmol/m^2)
	2180–2200	2220	2238	
	LAS concentration, μmol/g			
γ-(600°C)	495	–	–	495 (2.25)
γ_{boe}-(600°C)	225	–	–	225 (2.50)
χ-(600°C)	900	12	–	912 (3.51)
η-(600°C)	1125	20	24	1169 (3.70)
θ-(1000°C)	550	8	8	566 (5.34)

est concentration of Brønsted acid sites (BAS's), whereas η-Al_2O_3 is characterized by the lowest concentration of these sites.

It is well known that CO molecules form complexes with surface Lewis acid sites (LAS's) and BAS's, and the strength of the sites determines the increase in the frequency of their stretching vibrations. According to our experimental results (Table 2), one, two (γ- and χ-Al_2O_3), or three (η- and θ-Al_2O_3) types of LAS's, which are characterized by absorption bands at 2180–2200, 2220, and 2238 cm^{-1} and are due to the surface coordinatively unsaturated aluminum cations, occur on the surface of the oxides. The nature of the observed sites can be hypothetically related to the presence of the following structures on the surface: absorption bands at 2180–2200 cm^{-1} belong to the structural type Al_0; it is most likely that the absorption band at 2238 cm^{-1} belongs to the type Al_5 (in this case, the aluminum atom is bound to four oxygen atoms, and this structure can occur on the edge of crystallites). Sechenya et al. [37] believed that the strong LAS is a truncated tetrahedron Al_t; however, according to other data [38, 39], this LAS structure is unstable, and it cannot exist under real conditions.

A comparison of the oxides in terms of the concentration of acid sites indicates (Table 2) that the total surface concentration of LAS's (ΣLAS) per unit surface area increases from 2.25 to 3.7 μmol/m^2 in the order γ- → γ_{boe}- → χ- → η-Al_2O_3. A distinctive feature of η-Al_2O_3 is that it contains strong LAS's with ν(CO) = 2238 cm^{-1}, whose fraction is small. A change from η- to θ-Al_2O_3 does not lead to a change in the number of LAS's; only their concentration expressed in μmol/g decreases; the ΣLAS in homogeneous θ-Al_2O_3 is 5.34 μmol/m^2.

Another very important factor affecting the surface acidity of, for example, γ-Al_2O_3 is the precipitation conditions of the corresponding hydroxide. This effect was clearly pronounced in a study of the catalytic properties of γ-Al_2O_3 in ethanol dehydration.

CATALYTIC POPERTIES OF ALUMINUM OXIDE AND SYSTEMS BASED ON IT

Aluminum Oxide as a Catalyst for Ethanol Dehydration

According to Di Cosimo et al. [40], the dehydration of ethanol can occur at both acid (K_a) and basic

Table 3. Characteristics of aluminum oxide samples synthesized under different conditions

Samples	Hydroxide precipitation conditions: pH–T (°C)–τ (h)–precipitating agent	T_{calcin}, °C	Phase	Texture characteristics from the low-temperature adsorption of N_2		
				S_{BET}, m^2/g	V_{pore}, cm^3/g	d_{pore}, Å
Al_2O_3-1	7–70–3–$(NH_4)_2CO_3$	550	γ-Al_2O_3	301	1.01	135
Al_2O_3-2	9–70–3–($(NH_4)_2CO_3$ + NH_4OH)			304	0.46	60
Al_2O_3-3	9–70–3–NH_4OH			305	0.43	56

Table 4. Catalytic properties of aluminum oxide samples in the reaction of ethanol dehydration*

Sample	Catalyst weight, g	T = 370°C, τ = 0.3 s			
		$X_{C_2H_5OH}$, %	S		
			C_2H_4	Acetaldehyde	Diethyl ether
Al_2O_3-1	0.426	81.1	70.9	3.0	26.1
Al_2O_3-2	0.645	93.3	91.8	2.8	5.4
Al_2O_3-3	0.697	82.5	74.9	2.0	23.0
Al_2O_3-2	0.736	T = 370°C, τ = 0.60 s			
		96.2	94.9	4.0	1.2
	1.231	T = 370°C, τ = 1.21 s			
		99.7	95.3	4.6	0.1

* $X_{C_2H_5OH}$ is ethanol conversion, and S is selectivity.

(K_b) surface sites; however, the corresponding selectivities for the resulting products are different, as follows from the scheme given below.

Ethanol dehydration on acid and basic catalysts

$$CH_3CH_2OH \xrightarrow{K_a} CH_2CH_2 + H_2O$$

$$CH_3CH_2OH \xrightarrow{K_b} \tfrac{1}{2}CH_3CH_2OCH_2CH_3 + \tfrac{1}{2}H_2O \text{ (intermolecular dehydration)}$$

$$CH_3CH_2OH \xrightarrow{K_b} CH_3CHO + H_2 \text{ (dehydrogenation)}$$

Scheme.

Because aluminum oxide is a typical solid Lewis acid, we prepared aluminum oxide samples under different conditions. It can be seen (Table 3) that the given oxides have the same specific surface area of 300 m^2/g (the pore volume and the average pore diameter of Al_2O_3-1 were greater than those in the samples Al_2O_3-2 and Al_2O_3-3 by a factor of about 2).

The samples were tested in the above reaction, which was carried out in a flow reactor at a temperature of 370°C and a residence time of 0.3 s (Table 4). Table 4 indicates that the aluminum oxide sample Al_2O_3-2 was the most active and most selective for ethylene: at 93.3% ethanol conversion, the ethylene selectivity was 91.8%, whereas the conversion of ethanol on Al_2O_3-3 was 82.5% and the ethylene selectivity was 74.9%; the above oxides had almost identical texture characteristics (Table 3). Note that the selectivity of the reaction for diethyl ether on the tested samples differed by a factor of about 5: it was 5.4% for Al_2O_3-2 and 23–26% for Al_2O_3-1 and Al_2O_3-3; the selectivity for acetaldehyde was almost the same. The activity and selectivity of the reaction for ethylene can be increased by changing the residence time from 0.3 to 1.2 s; in this case, the almost complete conversion of ethanol is reached at 95.3% ethylene selectivity (Table 4).

With the above ethanol conversion scheme taken into account, it is likely that the observed differences in selectivity for dehydration products are due to the different surface acidities of the aluminum oxide samples. Indeed, an IR spectroscopic study of the samples confirmed this assumption. According to the experimental data (Table 5), the total concentration of OH groups decreased in the order Al_2O_3-1 → Al_2O_3-2 → Al_2O_3-3, and this order was also retained in terms of

Table 5. Positions of the absorption band maximums of OH groups in the IR spectra of aluminum oxide samples and their concentrations

Sample	ν(OH), cm^{-1}							ΣOH (C_t/C_b), μmol/g
	3660–3665	3670–3680	3700–3710	3730	3750	3773–3775	3790	
	Concentration of OH, μmol/g							
Al_2O_3-1	132	176	58	163	80	35	31	675 (146/529)
Al_2O_3-2	93	119	99	165	62	60	35	633 (157/476)
Al_2O_3-3	–	67	73	80	53	116	24	413 (193/220)

Table 6. Positions of the absorption bands of LAS's in the IR spectra of aluminum oxide samples and the concentrations of CO adsorbed on LAS's

Sample	ν(CO), cm^{-1}				ΣLAS, μmol/g (μmol/m^2)
	2185–2200	2205–2215	2220–2225	2237	
	LAS concentration, μmol/g				
Al_2O_3-1	625	7.2	4	–	636 (2.12)
Al_2O_3-2	810	60	9	3	882 (2.90)
Al_2O_3-3	695	–	–	–	695 (2.25)

the concentration of OH groups per surface square meter because it was the same in the samples under consideration (Table 3). The concentration of bridging OH groups in the test oxides also decreased in the above order (Table 5); therefore, Al_2O_3-1 was characterized by a higher Brønsted acidity.

Table 6 summarizes the concentrations of LAS's of different strengths and the total concentrations of LAS's. It can be seen that Al_2O_3-3 contained only weak LAS's (ν(CO) = 2185–2200 cm^{-1}); weak and medium-strength sites were present on the surface of Al_2O_3-1, whereas strong sites (ν(CO) = 2237 cm^{-1}) also occurred on the surface of Al_2O_3-2 in addition to the above sites; the total concentration of LAS's decreased in the order Al_2O_3-2 → Al_2O_3-3 → Al_2O_3-1. It is likely that the high total concentration of LAS's and the presence of strong LAS's on the surface of Al_2O_3-2 were responsible for the increased activity and selectivity of this oxide in ethanol dehydration.

Thus, changing the conditions of aluminum hydroxide precipitation makes it possible to prepare γ-alumina, which is characterized by the same specific surface area but different LAS strength and concentration distributions. Because of this, the activity and selectivity of oxides in ethanol dehydration are different. To obtain an effective catalyst for ethanol dehydration, a combination of a low concentration of BAS's and an increased concentration of LAS's, including strong LAS's (ν(CO) = 2237 cm^{-1}), is necessary.

Aluminum Oxide and Systems Based on It as Catalysts for the Ammonolysis of Propionitrile

Propionitrile ammonolysis, $C_2H_3N + NH_3 \rightarrow 2HCN + 2H_2$, is performed at high temperatures (700–800°C); therefore, the catalysts should be thermally stable and resistant to reduction, and they should possess sufficiently strong acid sites. For this very reason, aluminum oxides and systems based on them are of interest. Note that propionitrile ammonolysis is accompanied by the catalyst surface carbonization, $C_2H_3N \rightarrow [C_x] + nH_2 + mN_2$; therefore, the catalyst should have an optimum acid site strength distribution. Based on the assumption that use of binary systems with acid site strength and concentration distributions other than those in Al_2O_3 [19, 41] will make it possible to obtain a catalyst that meets the above requirements, we studied the systems based on aluminum oxide capable of essentially influencing both the target reaction of HCN production and the side reaction of surface carbonization.

Aluminum oxide and alumina-containing systems [42] were examined as catalysts. Tables 7 and 8 summarize the physicochemical properties of these systems. Aluminum oxide calcined at 1000°C is a mixture of δ- and θ-forms. The introduction of 5 mol % ZrO_2

Table 7. Phase compositions and specific surface areas of the synthesized alumina-containing catalysts [42]

Catalyst	M_nO_m, mol %	T_{calcin}, °C	Phase composition	S_{BET}, m^2/g
Al_2O_3	–	1000	δ- + θ-Al_2O_3	125
Al–Zr–O	5	700	γ-Al_2O_3, $D = 30$ Å	270
	40	700	γ-Al_2O_3: $a = 7.908$ Å, $D = 45$ Å;	
			ZrO_2 (tetragonal) + ZrO_2 (monoclinic) traces	230
Al–Mg–O	50	1100	$MgAl_2O_4$: $a = 8.081$ Å, $D = 100$ Å	60

Table 8. Acid properties of the synthesized catalysts [42]

Catalyst	M_nO_m, mol %	T_{calcin}, °C	Acidity × 10^6, mol/m^2				
			BAS	LAS			
				I	II	III	ΣLAS
Al_2O_3	–	1000	0.65	1.25	–	–	1.25
Al–Zr–O	5	700	0.25	3.03	0.047	0.056	3.13
	40	700	0.43	1.10	–	–	1.10
Al–Mg–O	50	1100	0.67	2.91	–	–	2.91

into Al_2O_3 followed by heat treatment at 700°C leads to the formation of fine-particle γ-Al_2O_3; the zirconium dioxide phase was not detected (Table 7). An increase in the fraction of ZrO_2 to 40 mol % is favorable for the formation of a complex phase composition: in addition to fine-particle γ-Al_2O_3, zirconium dioxide was present as a mixture of tetragonal and monoclinic modifications, and the latter was in a trace amount. The introduction of 50 mol % MgO into Al_2O_3 leads to the formation of aluminum–magnesium spinel, whose unit cell parameter almost coincides with the tabulated value [43]. The specific surface areas of the catalysts depend mainly on the temperature of their treatment. The catalysts calcined at 1000–1100 and 700°C have a specific surface area of 60–125 and 230–270 m^2/g, respectively (Table 7).

According to IR spectroscopic data (Table 8), the catalysts contain BAS's (ν(CO) = 2154–2159 cm^{-1}) and LAS's of different strengths: I, weak (ν(CO) = 2174–2193 cm^{-1}); II, medium-strength (ν(CO) = 2197–2200 cm^{-1}); and III, strong (ν(CO) = 2200–2208 cm^{-1}). Because the absorption bands of adsorbed CO are similar for individual oxides, in particular, aluminum and zirconium oxides, it is difficult to unambiguously assign particular absorption bands to the coordinatively unsaturated aluminum or zirconium cations.

Table 8 indicates that the concentration of BAS's decreases in the following order, depending on the nature of the catalyst: Al–Mg–O ≥ Al–O > Al–Zr(40)–O > Al–Zr(5)–O. Strong (III) and medium-strength LAS's (II) were observed only in Al–Zr(5)–O, and their concentration was low. The total concentration of LAS's changed in the following order, depending on the nature of the catalyst: Al–Zr(5)–O > Al–Mg–O > Al–O > Al–Zr(40)–O. Thus, the catalysts are characterized by different surface states, which can affect their catalytic properties and proneness to carbonization.

Figure 3 shows the dependence of propionitrile conversion and the amount of carbon formed on the catalyst surface on the catalyst on-stream time in propionitrile ammonolysis. The reaction was carried out in a flow system at 725°C and a constant composition of the reaction mixture: 2.0 ± 0.1 vol % propionitrile, 4.8 ± 0.2 vol % ammonia, and the balance helium (catalyst size fraction of 0.25–0.5 mm; reaction mixture flow rate of 10 L/h under normal conditions). As can be seen (Fig. 3a), the conversion of propionitrile decreases with on-stream time, whereas the fraction of carbon increases (Fig. 3b) and depends on the nature of the catalyst at comparable on-stream times. It is universally recognized that the deposited carbon blocks a portion of the surface to cause a decrease in catalytic activity. The experimental results suggest that the main reaction and the side carbonization reaction occur with the participation of the same active sites on the surface. This is confirmed by linear correlations (Fig. 4) between changes in the initial activity of the catalyst in the propionitrile ammonolysis reaction (evaluated from the specific first-order rate constant of the overall conversion of propionitrile) and the concentration of BAS's and, on the other hand, between the surface concentration of the formed coke and the concentration of BAS's.

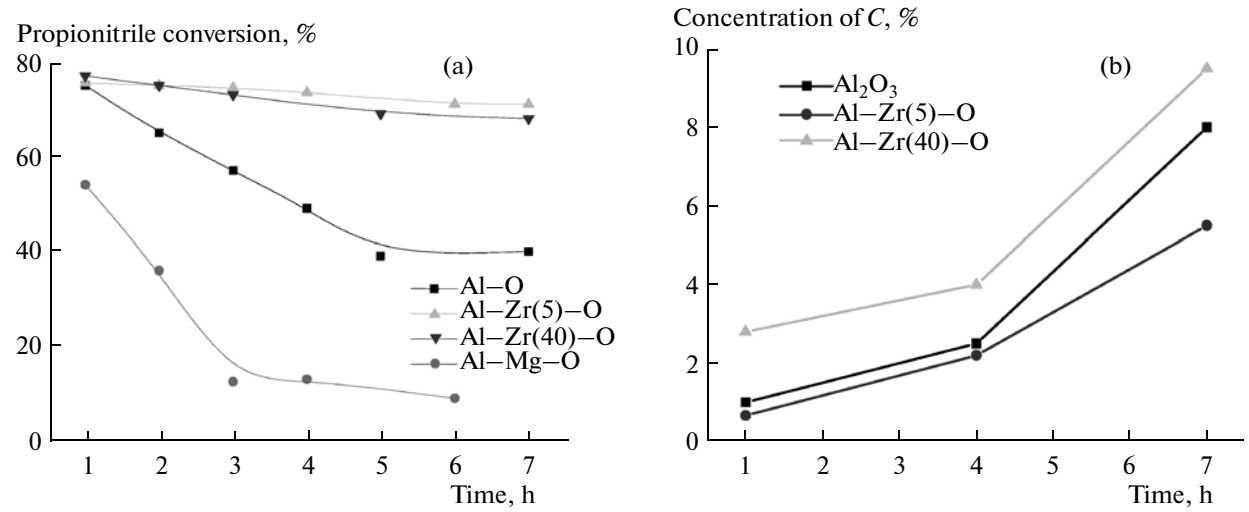

Fig. 3. (a) Propionitrile conversion and (b) the amount of carbon formed on the catalyst surfaces as functions of catalyst operation time.

Thus, the found correlations allow us to assume that the catalytic activity of catalysts based on aluminum oxide in the ammonolysis of propionitrile and their proneness to carbonization can be determined by the concentration of BAS's present on the surface. The conclusion about the participation of the above sites in both the main reaction and carbonization is consistent with data published by Ivanova et al. [44], who found that the formation of carbon on alumina–silica catalysts in acrolein condensation with ammonia is accompanied by a decrease in the fraction of OH groups bound to silicon.

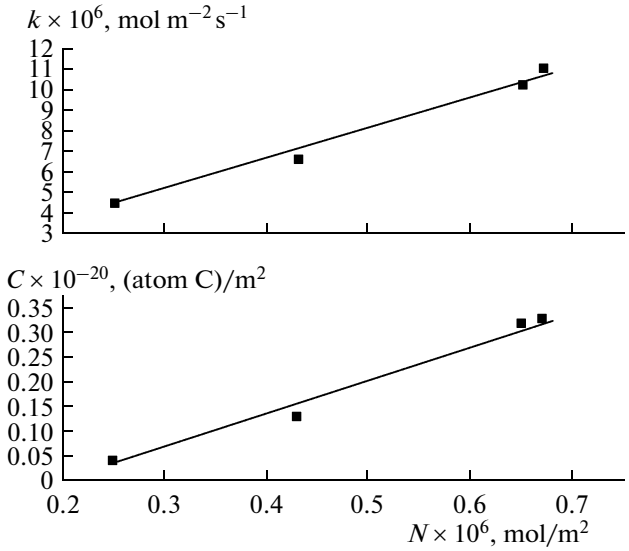

Fig. 4. Dependence of the specific first-order rate constant (k) of the overall conversion of propionitrile and the amount of carbon (C) deposited on the catalyst surface on the concentration (N) of BAS's.

Aluminum Oxide as a Support for a Manganese- and Bismuth-Containing Catalyst for Obtaining Nitrous Oxide by the Oxidation of Ammonia with Oxygen

Aluminum oxide is widely used as a support for different catalysts [45]. This is due to the facts that, firstly, aluminum oxide can exist in structurally different low-temperature and high-temperature forms; secondly, it contains surface LAS's, which exert a considerable effect on the distribution and state of the active component and, hence, on the catalytic activity; and, thirdly, it is characterized by an increased heat resistance [46]. For these reasons, Al_2O_3 was used as a catalyst support for the preparation of nitrous oxide by ammonia oxidation with oxygen.

It is well known [47, 48] that the oxidation of ammonia with oxygen can occur with the formation of molecular nitrogen, nitrogen oxide, or nitrous oxide. The target-oriented preparation of a specified product depends on both the nature of the catalyst and the process conditions. According to published and patent data [49–52], complex systems based on manganese dioxide are the most active and selective for N_2O in ammonia oxidation; the Mn–Bi–O binary composition occupies a special position among these systems. The bulk Mn–Bi–O composition is characterized by a relatively low degree of utilization of the active component; for this reason, the properties of supported Mn–Bi–O catalysts were studied.

γ-Al_2O_3 (S_{BET} = 200 m^2/g, V_Σ = 0.95 cm^3/g, and ρ = 0.62 g/cm^3) and α-Al_2O_3 (S_{BET} = 10 m^2/g, V_Σ = 0.40 cm^3/g, and ρ = 1.09 g/cm^3) were examined as supports. According to chemical analysis data (Table 9), the concentrations of manganese and bismuth oxides

Table 9. Physicochemical properties of manganese–bismuth oxide catalysts

Catalyst	T_{calcin}, °C (τ, h)	Active component				S_{BET}, m^2/g	Phase composition
		wt %		Mn/Bi	Σ(Mn + Bi), atom/nm^2		
		MnO_2	Bi_2O_3				
Mn–Bi–O/α-Al_2O_3	400(2)	13.0	9.0	1.01	75.1	10	MnO_2, $Bi(NO_3)_3$ (traces), α-Al_2O_3
	550(2)					8.7	β-MnO_2, β-Mn_2O_3, α-Bi_2O_3, α-Al_2O_3
	550(4)					8.0	β-MnO_2, β-Mn_2O_3, α-Bi_2O_3, $Bi_2Mn_4O_{10}$, α-Al_2O_3
	750(2)					7.5	β-Mn_2O_3, $Bi_2Mn_4O_{10}$, α-Al_2O_3
Mn–Bi–O/γ-Al_2O_3	400(2)	21.1	12.0	1.23	5.8	100	β-MnO_2, $Bi(NO_3)_3$ (traces), Bi_2O_3, γ-Al_2O_3
	550(2)					101	β-MnO_2, β- and α-Bi_2O_3, γ-Al_2O_3
	550(4)					103	β-MnO_2, Mn_2O_3, β- and α-Bi_2O_3, $Bi_2Mn_4O_{10}$, $Bi_2Al_4O_9$, γ-Al_2O_3
	750(2)					97	β-Mn_2O_3, $Bi_2Mn_4O_{10}$, $Bi_2Al_4O_9$, γ-Al_2O_3

supported on the above materials were different; however, the Mn/Bi ratio was ≥ 1 [53]. The surface concentration of the active components decreased upon the replacement of α-Al_2O_3 by γ-Al_2O_3; this was primarily due to the specific surface area of the latter.

The results of X-ray diffraction analysis showed (Table 9) that the resulting catalysts were multiphase: in addition to the support phase, they contained individual manganese and bismuth oxides and their interaction products. The Mn–Bi–O/α-Al_2O_3 catalysts calcined at 400°C contained MnO_2, undecomposed $Bi(NO_3)_3$ traces, and α-Al_2O_3. An increase in T or thermal treatment time τ favored the formation of β-Mn_2O_3, α-Bi_2O_3, and the reaction product $Bi_2Mn_4O_{10}$, and the fraction of this reaction product increased as the temperature was increased to 750°C (Table 9). The MnO_2 and Bi_2O_3 phases were not detected after treatment at 750°C. The Mn–Bi–O/γ-Al_2O_3 catalysts calcined at 400°C had approximately the same phase composition as Mn–Bi–O/α-Al_2O_3 (Table 9). The difference was that, firstly, the crystallization of individual (Bi_2O_3) phases was accelerated as a result of a higher concentration of the active component and, secondly, the support phase (γ-Al_2O_3) was characterized by a smaller unit cell parameter than the pure oxide [54]; this fact suggests the formation of a solid solution based on γ-Al_2O_3. A comparison of the ionic radii of aluminum (0.057 nm), bismuth ($r_{Bi3+} = 0.120$ nm), and manganese ($r_{Mn4+} = 0.052$, $r_{Mn3+} = 0.070$, and $r_{Mn2+} = 0.091$ nm) indicates that the aluminum oxide is promoted by manganese cations. Furthermore, the bismuth aluminate $Bi_2Al_4O_9$ forms as T and τ are increased in the heat treatment of the samples (Table 9). Thus, upon the supporting of an active component onto α-Al_2O_3, the components of the active phases interact to form $Bi_2Mn_4O_{10}$; with γ-Al_2O_3, not only the constituents of the active component but also the active component and the support interact to form $Bi_2Al_4O_9$.

The study of the catalytic properties of the synthesized catalysts showed (Fig. 5a) that the conversion of ammonia was almost independent of the nature of the support, and it decreased insignificantly as the T_{calcin} of the catalyst was increased. Another behavior was shown by the nitrous oxide selectivity: it can be seen (Fig. 5b) that the Mn–Bi–O/γ-Al_2O_3 catalyst was less selective than the Mn–Bi–O/α-Al_2O_3 catalyst by a factor of about 2; the selectivity decreased as the heat treatment temperature was increased. The observed differences between the nitrous oxide selectivities can be either due to the surface concentrations of the active component differing by more than an order of magnitude (Table 9) or due to the different phase compositions and different states of the active component,

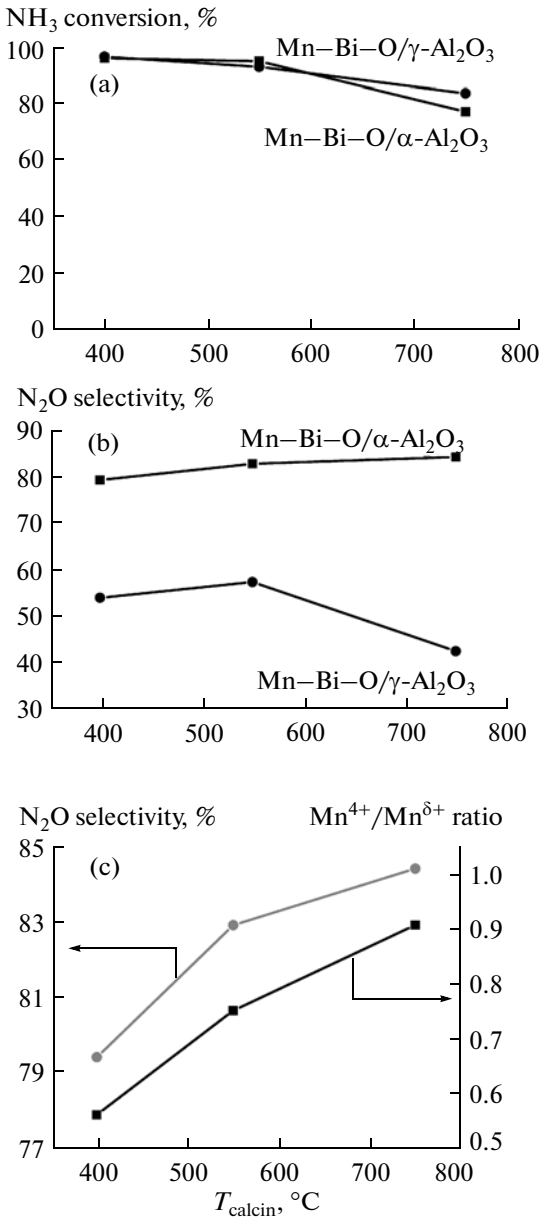

Fig. 5. (a) Ammonia conversion and (b) N_2O selectivity in the oxidation of ammonia with oxygen on the Mn–Bi–O/γ(α)-Al_2O_3 catalysts as functions of catalyst calcination temperature; (c) N_2O selectivity and the ratio between the fractions of oxidized and reduced manganese on the Mn–Bi–O/α-Al_2O_3 catalyst as functions of catalyst calcination temperature.

as suggested by the results of X-ray photoelectron spectroscopy (XPS) [53]. In accordance with these results, it was found (Fig. 5c) that there is a linear correlation between the dependences of the selectivity for nitrous oxide and the ratio between the fractions of oxidized and reduced manganese on the T_{calcin} of the catalyst. Consequently, it is believed that the oxidation of ammonia occurs through the step of adsorbed ammonia activation, which is accompanied by the reduction of $Mn^{4+(3+)}$ to Mn^{2+} followed by reoxidation with oxygen.

Aluminum Oxide as a Support for the Pd-Containing Active Component of a Catalyst for Carbon Monoxide Oxidation

Aluminum oxide, mainly γ-Al_2O_3, is frequently used as a support for noble metals. It is well known [55–58] that the redox properties of supported noble metals depend considerably on the nature of their interaction with the support. Otto and coauthors [57, 58] used XPS and Raman spectroscopy to demonstrate that palladium on the surface of Pd/γ-Al_2O_3 samples was in the following two states: PdO formed at [Pd] > 0.5 wt %, and a fine-particle oxide product of the reaction of palladium and aluminum oxide was formed at [Pd] < 0.5 wt % [57]. Similar results were obtained [59, 60] for the samples of Pd/γ-Al_2O_3 with a low palladium content. A similar situation was also noted for the Pt/γ-Al_2O_3 system [57, 61]: at low concentrations, the metal was in fine-particle, cluster form with particle sizes smaller than 2 nm, whereas large particles similar to Pt black were formed at high concentrations.

The hitherto published results did not elucidate the nature of the metal–support interaction in the Pd(Pt)/γ-Al_2O_3 systems. It is assumed that the interaction of Pd with Al_2O_3 can lead to the formation of a two-dimensional surface complex [62] and a palladium aluminate phase (through the fixation of active cations by the octahedral vacancies of the support) and to the stabilization of palladium as PdO_2 [63]. For this reason, Ivanova et al. [64] studied the effect of the T_{calcin} of the support and catalyst on the physicochemical and catalytic properties of the Pd/γ-Al_2O_3 catalysts for carbon monoxide oxidation.

Aluminum oxides prepared at 550 and 800°C, which were γ-Al_2O_3 with the unit cell parameter $a = 7.922$ Å, the crystallite size $D = 3.5–5.0$ nm, and a specific surface area of 300 and 160 m^2/g, respectively, were used as supports. The supporting of palladium (1.02 wt %) on the above aluminum oxide did not change its structure; furthermore, the palladium oxide and palladium metal phases were not detected by X-ray diffraction analysis (Fig. 6). It is likely that supported palladium was in the fine-particle state. Only an increase in the T_{calcin} of the catalysts to 1000 and 1200°C was accompanied by a change in their phase composition (Fig. 6). In the Pd/Al_2O_3(800)-1000 sample, a poorly crystallized phase of aluminum oxide, which was a transitional γ- → δ-Al_2O_3 phase, and PdO in trace amounts were observed. In the Pd/Al_2O_3(800)-1200 sample, α-Al_2O_3, corundum, was the main phase; PdO and Pd^0 were also present. The unit cell parameter of Pd^0 is 0.3891 nm (±0.0003 nm), which

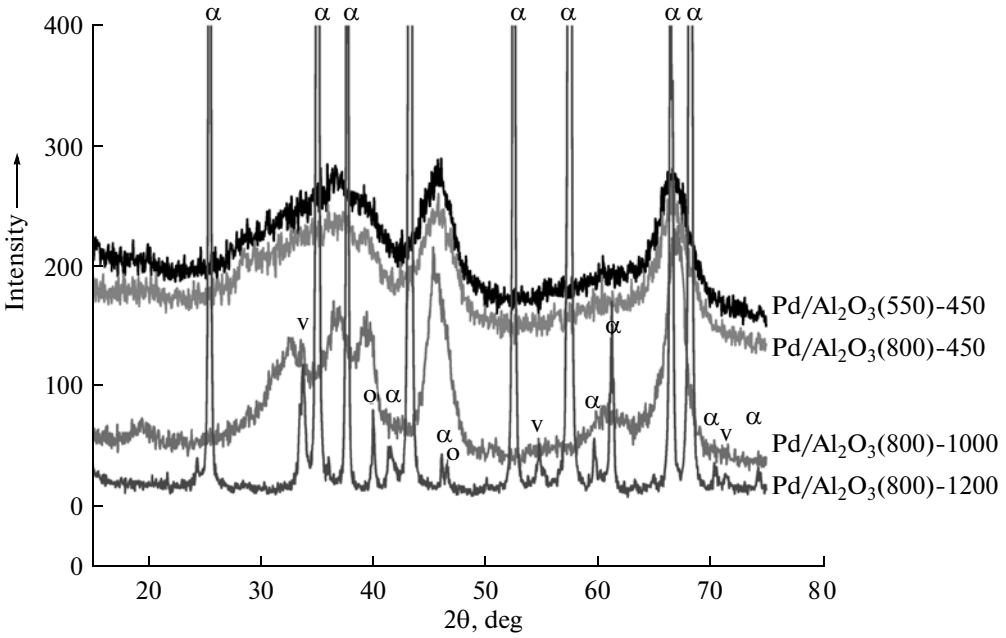

Fig. 6. Diffraction patterns of the $Pd/Al_2O_3(T_{supp})-T_{Cat}$ catalysts with different support and catalyst calcination temperatures. Notation: α is α-Al_2O_3; v is PdO; and o is Pd^0.

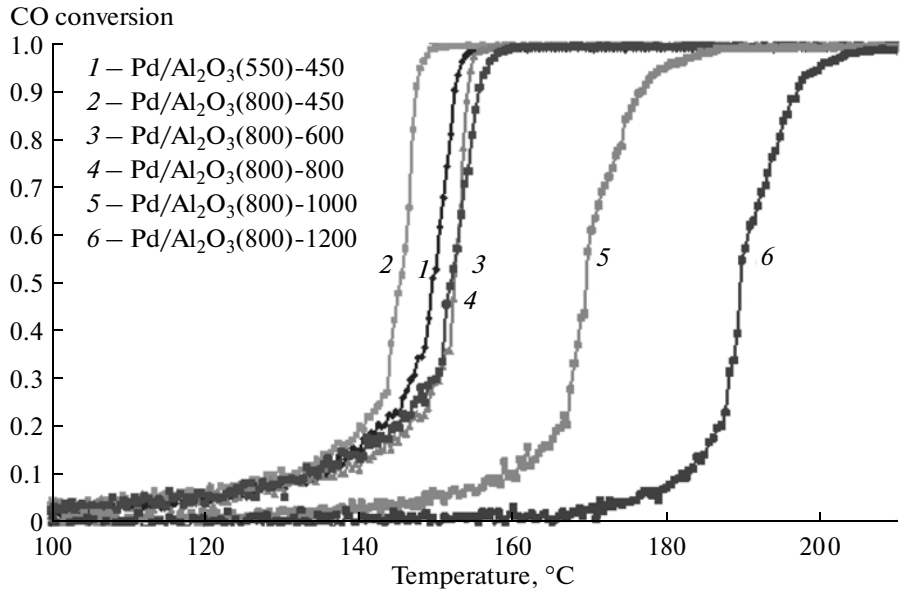

Fig. 7. Dependence of the conversion of CO upon reaction temperature on the samples $Pd/Al_2O_3(T_{supp})-T_{Cat}$ with different support and catalyst calcination temperatures.

almost coincides with the tabulated value (ICDD PDF2 No. 00-046-1043); the size of its particles is ~70 nm.

The testing of the catalysts in CO oxidation demonstrated (Fig. 7) that an increase in the T_{calcin} of the support at the same catalyst calcination temperature increased the activity of the catalyst, namely: T_{50} decreased from 150 to 145°C. The subsequent increase in the T_{calcin} of the catalyst was accompanied only by a decrease in the activity. The changes in the activity were due to the changes in both the particle sizes of palladium and the degree of its interaction with the support [64], which was confirmed by the results given below.

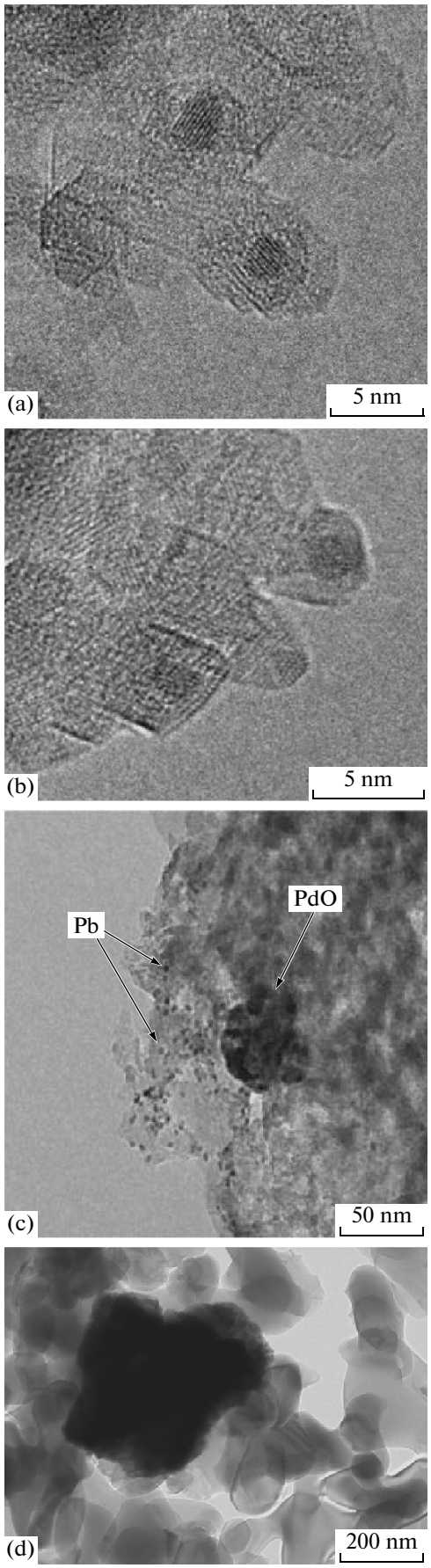

Fig. 8. High-resolution electron micrographs of the following catalysts: (a) $Pd/Al_2O_3(550)$-450, (b) $Pd/Al_2O_3(800)$-450, (c) $Pd/Al_2O_3(800)$-1000, and (d) $Pd/Al_2O_3(800)$-1200.

Firstly, according to electron microscopic data, palladium particles in $Pd/Al_2O_3(550)$-450 occurred both as single particles (2–3 nm), whose surface was almost completely covered with a thin layer of Al_2O_3, and as aggregates (≤100 nm) (Fig. 8a). An increase in the T_{calcin} of the support to 800°C did not exert a considerable effect on particle distribution, but it led to a decrease in the size of aggregated particles by a factor of 5–10 (Fig. 8b). The aggregated particles of Pd consisted of crystalline blocks of size 2–4 nm, which were joined at dislocation boundaries. Note that, in this catalyst, the greater part of the metal surface was covered with a layer of Al_2O_3; palladium was oxidized on the Pd/Al_2O_3 contact side, extending from the initial surface. An increase in the T_{calcin} of the Pd/Al_2O_3 catalyst to 1000°C led to the agglomeration of PdO aggregates, whereas small Pd^0 particles remained in a nanosized (2–3 nm) state as a result of their decoration with the support (Fig. 8c). The calcination of the Pd/Al_2O_3 catalyst at 1200°C facilitated, on the one hand, the subsequent agglomeration of PdO particles and, on the other hand, the reduction of large PdO particles to Pd^0 (Fig. 8d). The action of the reaction mixture was accompanied by the palladium oxidation–reduction processes with the formation of small palladium metal particles in the case of the $Pd/Al_2O_3(800)$-1000 sample and small palladium particles with the core–shell structure in the case of the $Pd/Al_2O_3(800)$-1200 sample.

Secondly, the character of catalysts reduction under conditions of temperature-programmed reduction (TPR) depended on the T_{calcin} of the support (Fig. 9). The TPR-H_2 profile of the $Pd/Al_2O_3(550)$-450 sample did not contain a clearly pronounced maximum; this fact suggests strong bonding between palladium and the support, and it is likely that the reduction of palladium occurs at higher temperatures. The TPR-H_2 curve of the $Pd/Al_2O_3(800)$-450 catalyst exhibited two peaks with maximums at 48 and 64°C. The presence of two peaks in the reduction of PdO was attributed to the presence of two oxide phases [65] differently interacting with the surface of the support. Smaller PdO particles more strongly interact with the support to cause an increase in the reduction temperature. Delage et al. [66] made the same conclusion and demonstrated that a more complicated reduction profile arose from different types of Pd–support interactions. However, because the absorbed H_2/Pd ratio for the test catalyst is 1.09, PdO is the main state of palladium on the support surface; consequently, the first and second peaks may be due to the reduction of palladium oxide aggregates and the reduction of oxide clusters, respectively.

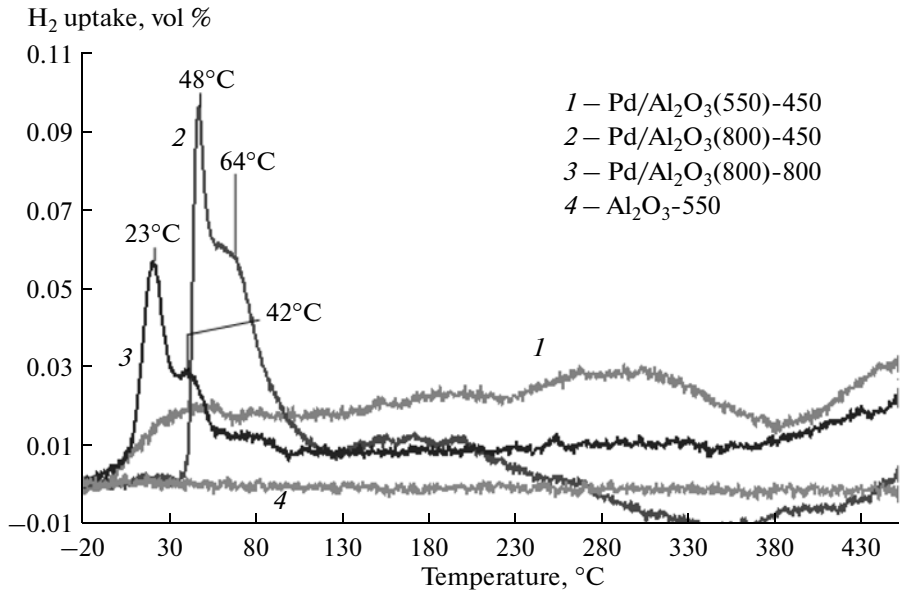

Fig. 9. TPR-H_2 profiles for the following catalysts with different support and catalyst calcination temperatures: (*1*) $Pd/Al_2O_3(550)$-450, (*2*) $Pd/Al_2O_3(800)$-450, (*3*) $Pd/Al_2O_3(800)$-800, and (*4*) γ-$Al_2O_3(550)$.

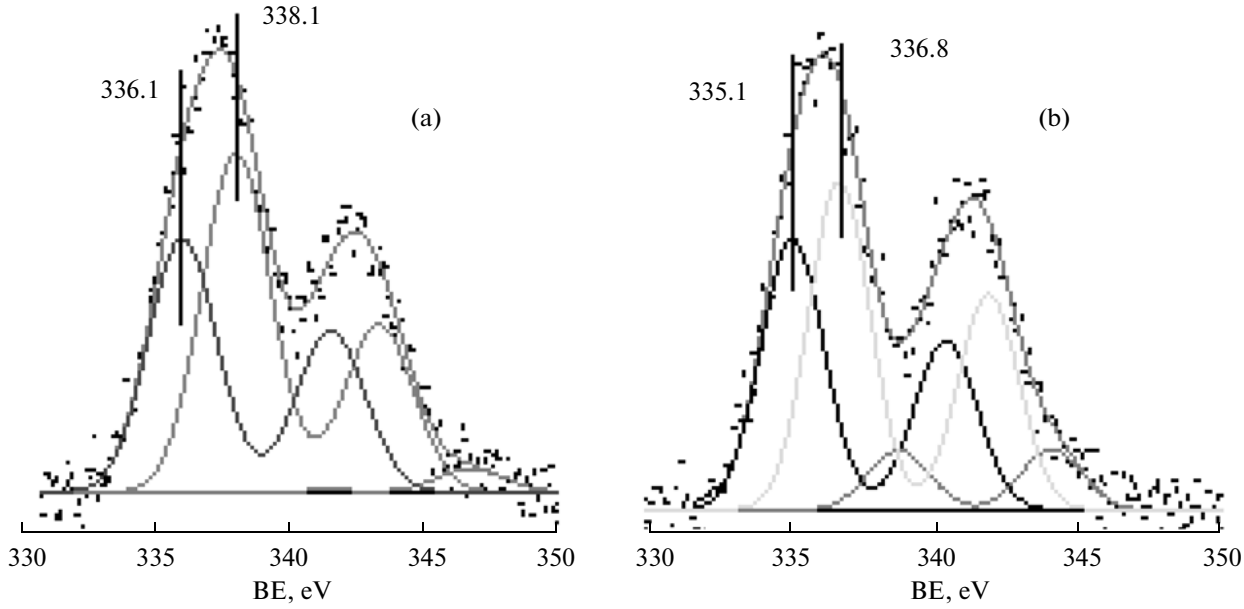

Fig. 10. Pd 3*d* XPS spectra of the (a) $Pd/Al_2O_3(550)$-450 and (b) $Pd/Al_2O_3(800)$-450 catalysts.

Thus, a decrease in the reduction temperature of palladium in $Pd/Al_2O_3(800)$-450, as compared with that in $Pd/Al_2O_3(550)$-450, suggests a smaller degree of palladium interaction with the support.

Thirdly, according to XPS data, a passage from $Pd/Al_2O_3(550)$-450 to $Pd/Al_2O_3(800)$-450 was accompanied by a decrease in the binding energy of the high-energy component in the Pd 3*d* spectra from 338.1 to 336.8 eV (Fig. 10); that is, different states of supported palladium were formed, depending on the T_{calcin} of the support. Consequently, the activity of Pd/Al_2O_3 catalysts in the oxidation of CO is determined by the particle size and state of palladium, which, in turn, depend on the particle size of the support.

Thus, the above results indicates that not only γ- but also α-aluminum oxide can be an effective catalyst and support for either oxide or metal active components owing to its structural, textural, and acid–base properties.

REFERENCES

1. Satterfield, Ch. N., *Heterogeneous Catalysis in Practice*, New York: McGraw-Hill, 1980.
2. Platonov, O.I. and Severilov, A.V., *CKatal. Prom–sti.,* 2003, no. 1, p. 22.
3. Misra, C., *Industrial Alumina Chemicals*, ACS Monograph 184, Washington, DC: Am. Chem. Soc., 1986.
4. Knözinger, H. and Ratnasamy, P., *Catal. Rev.*, 1978, vol. 17, no. 1, p. 31.
5. Ishchenko, E.D., Kim En-Khva, and Mustafina, M.K., in *"Nauchnye osnovy prigotovleniya i tekhnologii katalizatorov", Tezisy dokl. II Vses. soveshch.* (Proc. II USSR. Conf. on Catalyst Preparation and Technology), Minsk, 1989.
6. Pinec, H. and Haag, W.J., *J. Chem. Soc.*, 1961, vol. 83, no. 13, p. 2847.
7. Taylor, K.C., *Catal. Rev.*, 1993, vol. 35, p. 457.
8. Belton, D.N. and Taylor, K.C., *Curr. Opin. Solid State Mater. Sci.*, 1999, vol. 4, p. 97.
9. Nunan, J.G., *SAF Paper 970467*, 1997.
10. Fernandez-Garcia, M., Martinez-Arias, A., Conesa, J.C., and Soria, J., *Appl. Catal., B*, 2001, vol. 31, p. 39.
11. Martinez-Arias, A. and Fernandez-Garcia, M., *Appl. Catal., B*, 2001, vol. 31, p. 51.
12. Martinez-Arias, A. and Fernandez-Garcia, M., *Appl. Catal., B*,, 2002, vol. p. 151.
13. Ivanova, A.S., *Ind. Catal. Lectures*, 2009, no. 8, p. 7.
14. Dzis'ko, V.A., Ivanova, A.S., and Vishnyakova, G.P., *Kinet. Katal.*, 1976, vol. 17, no. 2, p. 483.
15. Lamberov, A.A., *Doctoral (Eng.) Dissertation*, Kazan: Kazan State Tech. Univ., 1999.
16. Alphonse, P. and Courty, M., *Thermochim. Acta*, 2005, vol. 425, p. 75.
17. *Physical and Chemical Aspects of Adsorbents and Catalysts*, Linsen, B.G., Ed., London: Academic, 1970.
18. Kul'ko, E.V., Ivanova, A.S., Kruglyakov, V.Yu., Moroz, E.M., Shefer, K.I., Litvak, G.S., Kryukova, G.N., Tanashev, Yu.Yu., and Parmon, V.N., *Kinet. Catal.*, 2007, vol. 48, no. 2, p. 316.
19. Ivanova, A.S., Litvak, G.S., Kryukova, G.N., Tsybulya, S.V., and Paukshtis, E.A., *Kinet. Catal.*, 2000, vol. 41, no. 1, p. 122.
20. Wolverton, C. and Hass, K.C., *Phys. Rev. B: Condens. Matter*, 2000, vol. 63, no. 2, p. 024102.
21. Smith, G.S. and Snyder, R.L., *J. Appl. Crystallogr.*, 1979, vol. 12, p. 60.
22. Halvarsson, M., Langer, V., and Vuorinen, S., *Surf. Coat. Technol.*, 1995, vols. 76–77, p. 358.
23. Ivanova, A.S., Litvak, G.S., Moroz, E.M., Kryukova, G.N., and Malakhov, V.V., *Izv. Sib. Otd. Akad. Nauk SSSR. Ser. Khim. Nauk*, 1990, no. 5, p. 62.
24. Ivanova, A.S., *Zh. Prikl. Khim.*, 1996, vol. 69, no. 11, p. 1790.
25. Kryukova, G.N., Klenov, D.O., Ivanova, A.S., and Tsybulya, S.V., *J. Eur. Ceram. Soc.*, 2000, vol. 20, no. 8, p. 1187.
26. Sato, T., *Thermochim. Acta*, 1985, vol. 88, no. 1, p. 69.
27. Kul'ko, E.V., Ivanova, A.S., Litvak, G.S., Kryukova, G.N., and Tsybulya, S.V., *Kinet. Catal.*, 2004, vol. 45, no. 5, p. 714.
28. Ivanova, A.S., Kulko, E.V., Litvak, G.S., Tsybulya, S.V., and Kryukova, G.N., *Abstr. EuropaCat VI*, Innsbruck, Austria, 2003, CD-ROM, B1.012.
29. Gates, B.C., Katzer, J.R., and Schuit, G.C.A., *Chemistry of Catalytic Processes*, New York: McGraw-Hill, 1979.
30. Oleshko, V.P., Lunina, E.V., Golubev, V.B., Bychkova, T.V., and Nekrasov, L.I., *Zh. Fiz. Khim.*, 1981, vol. 55, no. 5, p. 1160.
31. Paushtis, E.A., *IK-spektroskopiya v geterogennom kislotno-osnovnom katalize* (IR Spectroscopy Applied to Heterogeneous Acid–Base Catalysis), Novosibirsk: Nauka, 1992.
32. Peri, J., *J. Phys. Chem.*, 1965, vol. 69, no. 1, p. 220.
33. Digne, M., Sautet, P., Raybaud, P., Euzen, P., and Toulhoat, H., *J. Catal.*, 2002, vol. 211, p. 1.
34. Chukin, G.D., *Zh. Strukt. Khim.*, 1976, vol. 17, no. 1, p. 122.
35. Sun, M., Nicosia, D., and Prins, R., *Catal. Today*, 2003, vol. 86, nos. 1–4, p. 173.
36. Kul'ko, E.V., Ivanova, A.S., Budneva, A.A., and Paukshtis, E.A., *Kinet. Catal.*, 2005, vol. 46, no. 1, p. 132.
37. Sechenya, I.N., Chuvylkin, N.D., and Kazanskii, V.B., *Kinet. Katal.*, 1986, vol. 27, no. 3, p. 608.
38. Danyushevskii, V.G., *Konformatsionnyi analiz organicheskikh molekul* (Conformation Analysis of Organic Molecules), Moscow: Khimiya, 1982.
39. Bokii, G.B., *Kristallokhimiya* (Crystal Chemistry), Moscow: Nauka, 1971.
40. Di Cosimo, J.I., Diez, V.K., Xu, M., Iglesia, E., and Apesteguia, C.R., *J. Catal.*, 1998, vol. 178, p. 499.
41. Lunina, E.V., *Kataliz: Fundamental'nye i prikladnye issledovaniya* (Catalysis: Fundamental and Applied Research), Moscow: Mosk. Gos. Univ., 1987.
42. Ivanova, A.S., Bondareva, V.M., Bobrin, A.S., Litvak, G.S., Paukshtis, E.A., Chuvilin, A.L., and Noskov, A.S., *React. Kinet. Catal. Lett.*, 2005, vol. 84, no. 1, p. 143.
43. *ASTM Diffraction Data Cards and Alphabetical and Grouped Numerical Index of X-Ray Diffraction Data*, Philadelphia: ASTM, 1967.
44. Ivanova, A.S., Al'kaeva, E.M., Mastikhin, V.M., Paukshtis, E.A., and Kryukova, G.N., *Kinet. Catal.*, 1996, vol. 37, no. 3, p. 425.
45. Oberlander, R.K., in *Applied Industrial Catalysis*, Leach, B.E., Ed., New York: Academic, 1984, vol. 3, p. 63.
46. Wang, Ch.-B., Lee, H.-G., Yeh, T.-F., Hsu, S.-N., and Chu, K.-S., *Thermochim. Acta*, 2003, vol. 401, p. 209.
47. Bosh, H. and Jansen, F., *Catal. Today*, 1988, vol. 2, no. 4, p. 369.
48. Parvulescu, V.I., Grange, P., and Delmon, B., *Catal. Today*, 1998, vol. 46, no. 4, p. 233.
49. Czechoslovak Patent 158091, 1973.
50. *Kataliticheskie svoistva veshchestv: Spravochnik* (Catalytic Properties of Materials: A Handbook), Roiter, V.A., Ed., Kiev: Naukova Dumka, 1968.
51. Eur. Patent 0799792, 1997.
52. RF Patent 2102135, 1998.

53. Ivanova, A.S., Slavinskaya, E.M., Mokrinskii, V.V., Polukhina, I.A., Tsybulya, S.V., Prosvirin, I.P., Bukhtiyarov, V.I., Rogov, V.A., Zaikovskii, V.I., and Noskov, A.S., *J. Catal.*, 2004, vol. 221, no. 1, p. 213.

54. Ivanova, A.S., Skripchenko, E.V., Moroz, E.M., Litvak, G.S., Kustova, G.N., and Krivoruchko, O.P., *Izv. Sib. Otd. Akad. Nauk SSSR*, 1989, no. 6, p. 116.

55. Ciuparu, D. and Pfefferle, L., *Appl. Catal., A*, 2001, vol. 209, nos. 1–2, p. 415.

56. Rodriguez, N.M. Oh, S.G., Dallabetta, R.A., and Baker, R.T.K., *J. Catal.*, 1995, vol. 157, no. 2, p. 676.

57. Otto, K., Haack, L.P., and de Vries, J.E., *Appl. Catal., B*, 1992, vol. 1, no. 1, p. 1.

58. Otto, K., Hubbard, C.P., Weber, W.H., and Graham, G.W., *Appl. Catal., B*, 1992, vol. 1, no. 4, p. 317.

59. Goetz, J., Volpe, M.A., Sica, A.M., Gigola, C.E., and Touroude, R., *J. Catal.*, 1995, vol. 153, no. 1, p. 86.

60. Sandoval, V.H. and Gigola, C.E., *Appl. Catal., A*, 1996, vol. 148, no. 1, p. 81.

61. Yao, H.C., Sleg, M., and Phunmer, H.K., *J. Catal.*, 1979, vol. 59, p. 365.

62. Hoost, T.E. and Otto, K., *Appl. Catal., A*, 1992, vol. 92, p. 39.

63. Lesage-Rosenberg, E., Vlaic, G., Dexpert, H., Lagarde, P., and Freund, E., *Appl. Catal.*, 1986, vol. 22, p. 211.

64. Ivanova, A.S., Slavinskaya, E.M., Gulyaev, R.V., Zaikovskii, V.I., Danilova, I.G., Plyasova, L.M., Polukhina, I.A., and Boronin, A.I., *Appl. Catal., B*, 2010, vol. 97, nos. 1–2, p. 57.

65. Sales, E.A., Jove, J., Mendes, M.J., and Bozon-Verduraz, F., *J. Catal.*, 2000, vol. 195, p. 88.

66. Delage, M., Didillon, B., Huiban, Y., Lynch, J., and Uzio, D., *Stud. Surf. Sci. Catal.*, 2000, vol. 130, no. 2, p. 1019.